Journal of Power Sources 261 (2014) 363–370

Contents lists available at ScienceDirect

Journal of Power Sources

journal homepage: www.elsevier.com/locate/jpowsour

Porous carbon materials for Li–S batteries based on resorcinol–formaldehyde resin with inverse opal structure

Mukesh Agrawal [a,*,1], Soumyadip Choudhury [a,b], Katharina Gruber [c], Frank Simon [a], Dieter Fischer [a], Victoria Albrecht [a], Michael Göbel [a], Stefan Koller [c], Manfred Stamm [a,b], Leonid Ionov [a,*]

[a] Leibniz-Institut für Polymerforschung Dresden e.V., Hohe Str. 6, 01069 Dresden, Germany
[b] Technische Universität Dresden, Physical Chemistry of Polymer Materials, 01062 Dresden, Germany
[c] VARTA Micro Innovation GmbH, Graz, Austria

HIGHLIGHTS

- Thorough investigation of porous carbon with inverse opal-like structure.
- Thorough electrochemical characterization of porous carbon as material for Li–S batteries.
- Very high initial charging/discharging capacity.

ARTICLE INFO

Article history:
Received 23 January 2014
Received in revised form
6 March 2014
Accepted 14 March 2014
Available online 24 March 2014

Keywords:
Energy storage
Lithium sulfur batteries
Carbon
Cathode
Sulfur

ABSTRACT

This study reports on a novel approach to fabrication of carbon-sulfur composite material and demonstrates its application as cathode for Li–S batteries. Firstly, highly porous carbon material has been prepared by exploiting PMMA colloidal crystal arrays as sacrificial template and subsequently mixing with elemental sulfur at 155 °C. The resulting carbon-sulfur composite cathode material possess very high intrinsic surface area, conductivity and has been found to demonstrate as high as 1600 mAh g^{-1} capacity in 1st discharge cycle and about 300–400 mAh g^{-1} in 50th discharge cycle.

1. Introduction

Development of methods for storage of electrical energy have become highly important in recent time [1–3]. Two main general approaches for reversible storage of electric energy are commonly used. First one is supercapacitors [3], where energy is stored in the form of an electric double layer. In the second approach, the energy is stored in the form of chemical energy in rechargeable batteries [4]. While the supercapacitors allow higher power density, the rechargeable batteries are able to provide higher energy density. Among all variety of rechargeable batteries, ones based on lithium deserve particular attention [5,6]. In fact, lithium is the lightest metal and has the highest oxidation potential among the metals that allows much higher energy density comparing, for example, to Ni–Cd rechargeable batteries. Currently, Li-ion batteries based on $LiMn_2O_4$ and $LiCoO_2$ cathodes are practically used [7–10]. These Li-ion batteries provide good cycling and very high columbic efficiency. On the other hand, they suffer from insufficient energy density. For example, the distance which can be traveled by the car equipped with Li-ion battery is 60–160 km, which in many cases is insufficient for everyday use. Li–S batteries are the emerging class of rechargeable batteries, which potentially can provide much higher energy density [11–14]. Although the lithium-sulfur system

* Corresponding authors.
E-mail addresses: mukeshiitd@gmail.com (M. Agrawal), ionov@ipfdd.de (L. Ionov).
[1] Present address: General Electric Plastics, John F. Welch Technology Centre, Bangalore, India.

http://dx.doi.org/10.1016/j.jpowsour.2014.03.052
0378-7753/

operates at a comparably low average potential of 2.1 V against Li^+/Li, it shows a high theoretic specific energy of 2600 Wh kg^{-1} due to the extraordinary theoretical specific capacity of 1675 mAh g^{-1} of sulfur.

The essential element of Li–S batteries is the sulfur cathode. Sulfur itself is electrically insulating and therefore composite cathodes, which consist of sulfur and porous conductive materials such as carbon, are used. Different carbon materials including acetylene black [15,16], carbon nanotubes [17,18], graphene [19,20], CMK-3 [21,22] and microporous activated carbon fibers [23] were used as conductive component [8,9,24]. Typically, these carbon materials are powders, which consist of grains with certain size. The surface area of these materials is controlled by the size of the grains and internal surface area of the grains. Very recently, polymers were introduced as precursors for design of porous carbon cathodes. Due to their flexibility, polymers may be used for fabrication of carbon materials with various micro and nanomorphology. For example, carbonization of polyacrylonitrile (PAN) mixed with Na_2CO_3 [25], poly(methyl methacrylate) (PMMA) – PAN blends [26], polymer fibers prepared by electrospinning [27], polypyrrole [28], sucrose [29], formaldehyde-phenol resin mixed with tetraethyl orthosilicate [30], hollow carbon capsules [31], nanoporous carbon [32,33], wrapping S by graphene particles which contain polyethylene glycol (PEG) [34] and use of porous carbon containing PEG [21], were used to prepare porous cathodes for Li–S batteries. Due to interconnectivity of pores and carbon phase as well as large surface area, opal and inverse-opal structures deserve particular interest as candidate for possible carbon structure. For example, Nazar et al. fabricated opal-like porous carbon structure using PMMA particles as template which was filled with SiO_2 and PMMA was replaced by CMK-3 carbon [35]. Inverse-opal like carbon structures were also prepared by carbonization of poly(furfuryl alcohol) and demonstrated very good cycling properties [36]. The advantages of opal-like porous carbon are following: (i) simplicity in fabrication; (ii) size and distribution of pores are well defined and controlled by the size of the particles. In this paper we report design of porous cathodes for Li–S batteries with inverse opal structure [37–40] using carbonized resorcinol–formaldehyde resin.

2. Experimental part

2.1. Materials

PMMA particles (10 wt% 490 nm, 740 nm diameter) were purchased from Microparticles GmbH. Resorcinol, formaldehyde solution (37%), sodium carbonate, sulfur, *N*-methyl-2-pyrrolidone were procured from Sigma Aldrich (Germany) and used as received without any further purification. PVDF (polyvinylidene fluoride) was purchased from CREAVIS Technologies and Innovation (DEGUSSA). Lithium foil was purchased from Kyokuto Metal Co. Nickel foil was purchased from Schlenk Metallfolien GmbH. Super P® Li conductive carbon black was obtained from TIMCAL Graphite and Carbon.

2.2. Preparation of porous carbon samples

Aqueous dispersions of PMMA particles (10 wt% solid content) were centrifuged to remove supernatant water and then dried under vacuum to get the PMMA colloidal crystal arrays. The calculated amount of the colloidal crystal arrays were subjected to the vacuum for 2 h to remove air from interstitial spaces and to facilitate the filling of carbon precursor (here resorcinol–formaldehyde resin) in to the free spaces in the colloidal crystal arrays. The resorcinol–formaldehyde resin was prepared by dissolving resorcinol in formaldehyde (37% formalin solution) in 1:1.8 molar ratio catalyzed by 0.56 mmol 10 wt% (w/w) sodium carbonate aq. solution. Afterwards the resorcinol–formaldehyde resin was injected in to the piece of colloidal crystal arrays in the low molecular state (i.e. when it was very fluid and crosslinking was not yet started) and it was soaked in resorcinol–formaldehyde resin for another 2 h. The soaked colloidal crystal slowly turned light brown. The light brown colored colloidal crystal powder soaked with resin-solution was heat treated at 85 °C for 2 days in a closed vessel and then for 12 h in an open vessel in an oven. Finally, the crosslinked material was pyrolyzed at 900 °C for 2 h at a programmed heating rate of 5 °C min^{-1} in an argon environment. After completion of pyrolysis a black piece of material was obtained which was ground in a mortar to get porous carbon powder to be used to blend with sulfur. All the characterization techniques for carbon as material were performed with this black brittle powder.

2.3. Fabrication of carbon-sulfur composite

Porous carbon material was pre-mixed with sulfur powder in a mortar in 1:2 w/w ratio in a mortar followed by mixing in a ball mill for even intensive mixing and subsequently heat treated at 155 °C for 5 h in an oven operated under argon. Heat treatment at 155 °C was done to facilitate the pore coverage by sulfur in to the entire available surface area of carbon. At 155 °C sulfur attains the minimum viscosity and molten sulfur makes a uniform coating over the carbon surfaces. As both of the components in the composite are hydrophobic in nature, so an easy and uniform mixing was achieved. Resulting material after thermal annealing (carbon–sulfur composite, 82 wt%) was further blended in ball mill with desired weight ratio of Super P® Li conductive carbon black (10 wt%) to aid the good contact between carbon and sulfur. The resulting material was used for the preparation of cathode material for Li–S batteries.

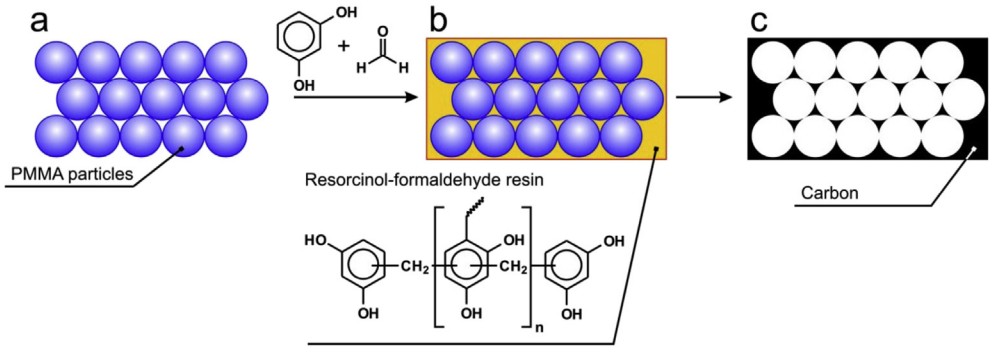

Fig. 1. Scheme of preparation of porous carbon. PMMA particles are assembled in opal-like structure (a), the PMMA-particle opal is filled with resorcinol formaldehyde resin (b). High temperature annealing results in decomposition of PMMA particles and carbonization of the resin (c).

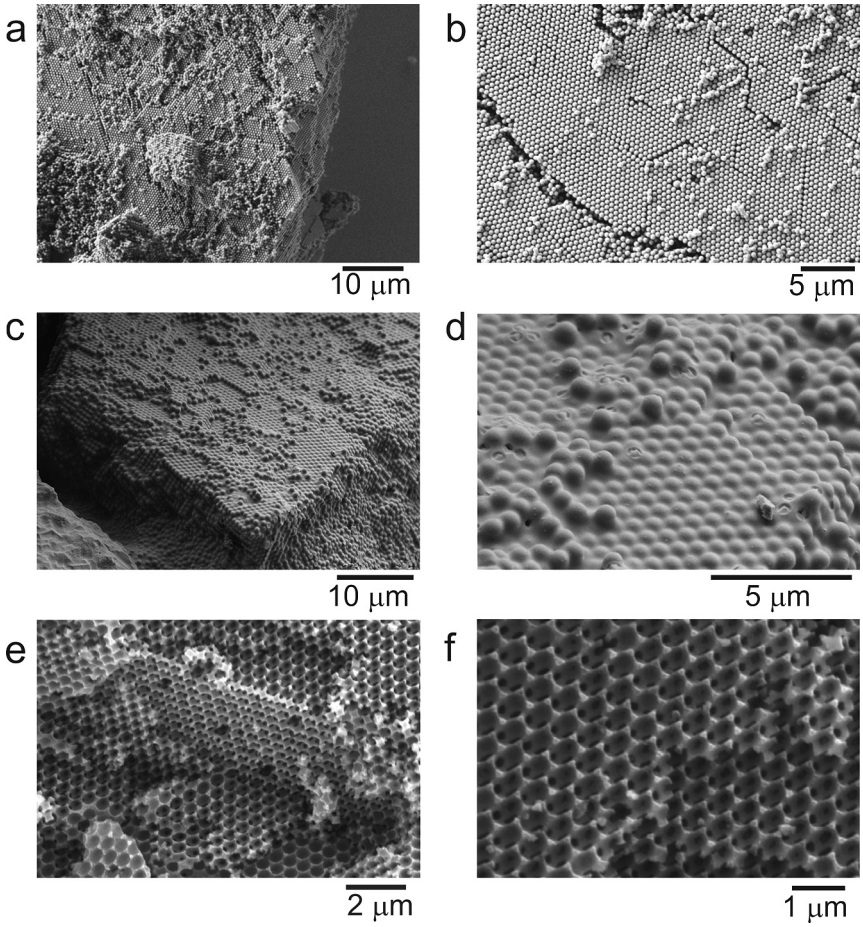

Fig. 2. SEM images of colloidal crystal formed by 490 nm large PMMA particles (a,b), colloidal crystal filled with resorcinol–formaldehyde resin (c,d), carbonized inverse opal (e,f). SEM images of structures obtained from 740 nm large PMMA beads are not shown but looks similar.

2.4. BET surface area measurements

Nitrogen adsorption at the temperature of liquid nitrogen (77 K) carried out according to Brunauer, Emmett, and Teller has been established as standard method to determine specific surface area (BET method). For the low-temperature gas adsorption was carried out employing the automatically working sorptiometer Autosorb-1 (Quantachrome GmbH & Co. KG, Odelzhausen, Germany), which is a volumetrically operating instrument. From the hysteresis between the recorded adsorption and desorption isotherms the pore

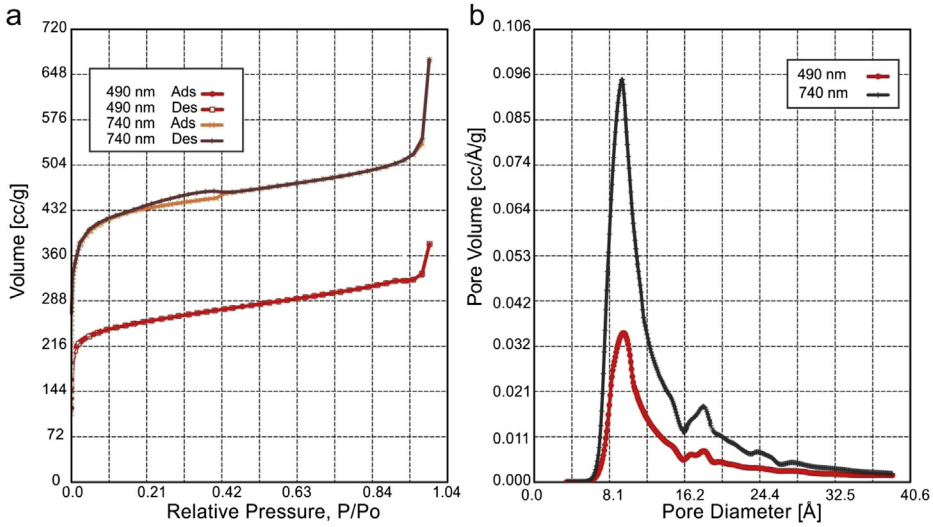

Fig. 3. Nitrogen adsorption–desorption isotherms at 77 K (a) and pore distribution of porous carbons obtained using particles of different size.

sizes of meso and micro pores (pore radii between 1 and 50 nm) and pore size distributions were determined according to the Barrett–Joyner–Halenda (BJH) and Saito-Foley (SF) methods.

2.5. X-ray photoelectron spectroscopy

XPS studies were carried out by means of an AXIS ULTRA photoelectron spectrometer (Kratos Analytical, Manchester, UK). The spectrometer was equipped with a monochromatic Al Kα X-ray source of 300 W at 15 kV. The kinetic energy of the photoelectrons was determined with a hemispheric analyzer set to pass energy of 160 eV for wide scan spectra and 20 eV for high-resolution spectra. During all measurements electrostatic charging of the sample was overcompensated by means of a low-energy electron source working in combination with a magnetic immersion lens. Later, all recorded peaks were shifted by the same amount which was necessary to set the C 1s peak to 284.00 eV for carbon atoms involved in the graphite-like lattice. Quantitative elemental compositions were determined from peak areas using experimentally determined sensitivity factors and the spectrometer transmission function. Spectrum background was subtracted according to Shirley [48]. The high-resolution spectra were deconvoluted by means of a computer routine (Kratos Analytical, Manchester, UK). Free parameters of component peaks were their binding energy, height, full width at half maximum and the Gaussian–Lorentzian ratio.

2.6. Scanning electron microscopy

Scanning electron microscopy (SEM) images were taken on a NEON40 microscope (Carl Zeiss Microscopy GmbH, Oberkochen, Germany) at an accelerating voltage of 3 kV. Samples were prepared by fixing a small piece of sample with a double-sided adhesive tape on a stub. In order to increase the contrast and quality of images, the samples were sputter coated with a 3 nm layer of platinum prior to analysis. SEM images were taken by using the Inlens and Everhart-Thornley detector.

2.7. Transmission electron microscopy

Transmission electron microscopy (TEM) and energy filtered imaging (EFTEM) were done on Libra 200 transmission electron microscope (Carl Zeiss Microscopy GmbH) operated at 200 keV. The specimen was prepared by dispersing carbon-sulfur powder in ethanol followed by placing a drop on a holey carbon film TEM grid. The TEM grid was dried at 50 °C to remove all traces of ethanol before TEM investigation.

2.8. Energy dispersive X-ray spectroscopy

The energy dispersive X-ray (EDX) measurements were made in Ultra Plus (Carl Zeiss Microscopy GmbH) scanning electron microscope (SEM) and a Quantax XFlash® QUAD 5060F EDX detector (Bruker Nano GmbH, Berlin, Germany). A primary beam of 5 keV was used for these measurements. Some sample grains were mounted on a double sided adhesive carbon tape.

Table 1
Specific surface area of porous carbon obtained using particles with different size.

Diameter of particles, nm	Surface area, $m^2\ g^{-1}$	
	Theoretical	Experimental (BET)
490	1743	700
740	1154	1340

Table 2
Conductivity values of different carbons.

Sample	Conductivity values ($mS\ cm^{-1}$)
Carbon prepared using 740 nm large particles	594.6
Carbon prepared using 490 nm large particles	998
Super P 65	3785.7
MPC- Sigma	Non conductive

2.9. Raman spectroscopy

The Raman-spectra was recorded using the confocal Raman microscope alpha 300 R (WITec GmbH, Ulm, Germany) equipped with a laser with an excitation wavelength of 532 nm. The samples were analyzed with a 20× objective and an integration time of 0.5 s. The laser power was 5 mW. To improve the signal to noise ratio 200 accumulations were done. For a better comparison, each spectrum was normalized to the highest peak in the range from 300 to 3600 cm^{-1}. The samples were place on glass slides during Raman measurements.

2.10. Cyclic voltammetric and constant current measurements

Cathode slurry of desired viscosity was prepared by adding carbon-sulfur composite material (82 w%),blended with, Super P® Li (10 w%) conducting additive (carbon black) in a solution of PVdF in N-Methyl-2-pyrrolidone (8 wt% with respect to 82 wt% of carbon-sulfur composite) with a magnetic stirrer. The role of Super P® Li ion battery grade carbon black as additive is to provide better electric contact between particles of synthesized porous carbon sulfur composite by reducing the interparticle resistance of sulfur. A thin layer of the as prepared slurry was coated on nickel foil (60–

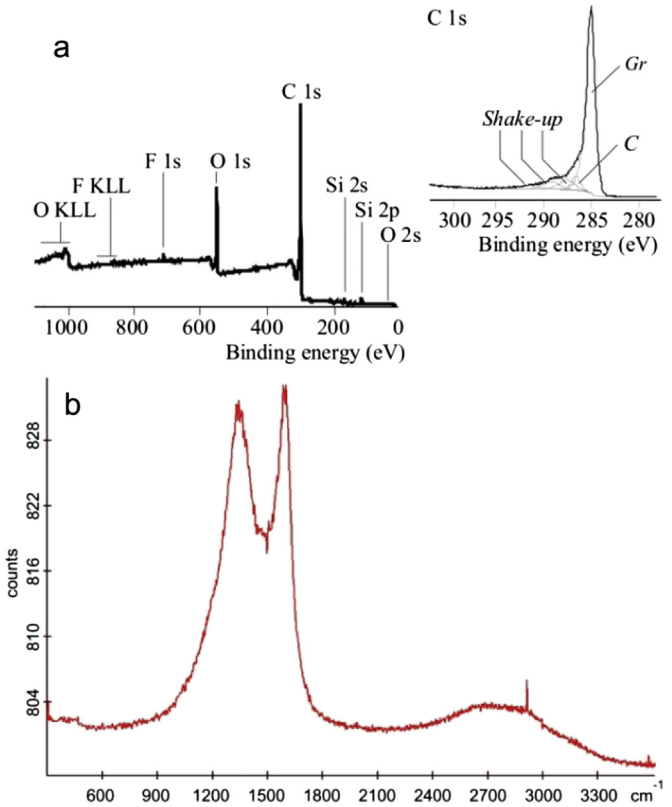

Fig. 4. Survey (a) and high resolution (inset in a) C 1s XPS spectra as well as RAMAN (b) spectra of carbonized resorcinol–formaldehyde resin measured for 490 nm sample.

80 μm wet thickness) and dried at 60 °C for 12 h. Resulting electrodes had a mass load of 0.40 mg cm^{-2} in dry state and a sulfur content of 55 wt%. A Swagelok® T-cell was used as testing device. Carbon-sulfur composite electrode served as working electrode, lithium metal served as counter and reference electrode respectively. 1 M solution of lithium bis(trifluoromethane sulfonyl)imide (LiTFSI) in a mixture of 1,2-Dimethoxyethane/1,3-Dioxolane (1/1, v/v)) was used as electrolyte, which was used to soak the nonwoven polypropylene separator during cell assembly. The cyclovoltammetric and the charge/discharge measurements were recorded using a Biologic MPG-2 and a Maccor Series 4000 battery tester respectively. For recording the CVs the vertex potentials were set to 1 V and 3.2 V vs. Li/Li^+ and the scan rate was set to 30 μV s^{-1}. For constant current measurements the vertex potentials were set to 1.5 V and 3.0 V vs. Li/Li^+ with a C-rate of 0.1.

2.11. Measurement of conductivity

The conductivity of the carbon samples in powder form was measured in built-in-house device and custom- made software. The carbon sample was ground to a powdery form in a ball mill prior to measurement. The powder to be examined was filled into a hollow PMMA cylinder and compressed by a piston. The PMMA hollow cylinder has cavity diameter of 5 mm separated by two gold electrodes that exactly fit into the cavity. One of the gold electrodes is stationary and the other one approaching towards the stationary end. Each time of measurement 50 mg of carbon powder was used. After filling the carbon powder in the cavity the upper gold electrode approach towards electrode and at the time of contact it shows the decrease of the resistivity. During the compression process, the electrical resistance was continuously

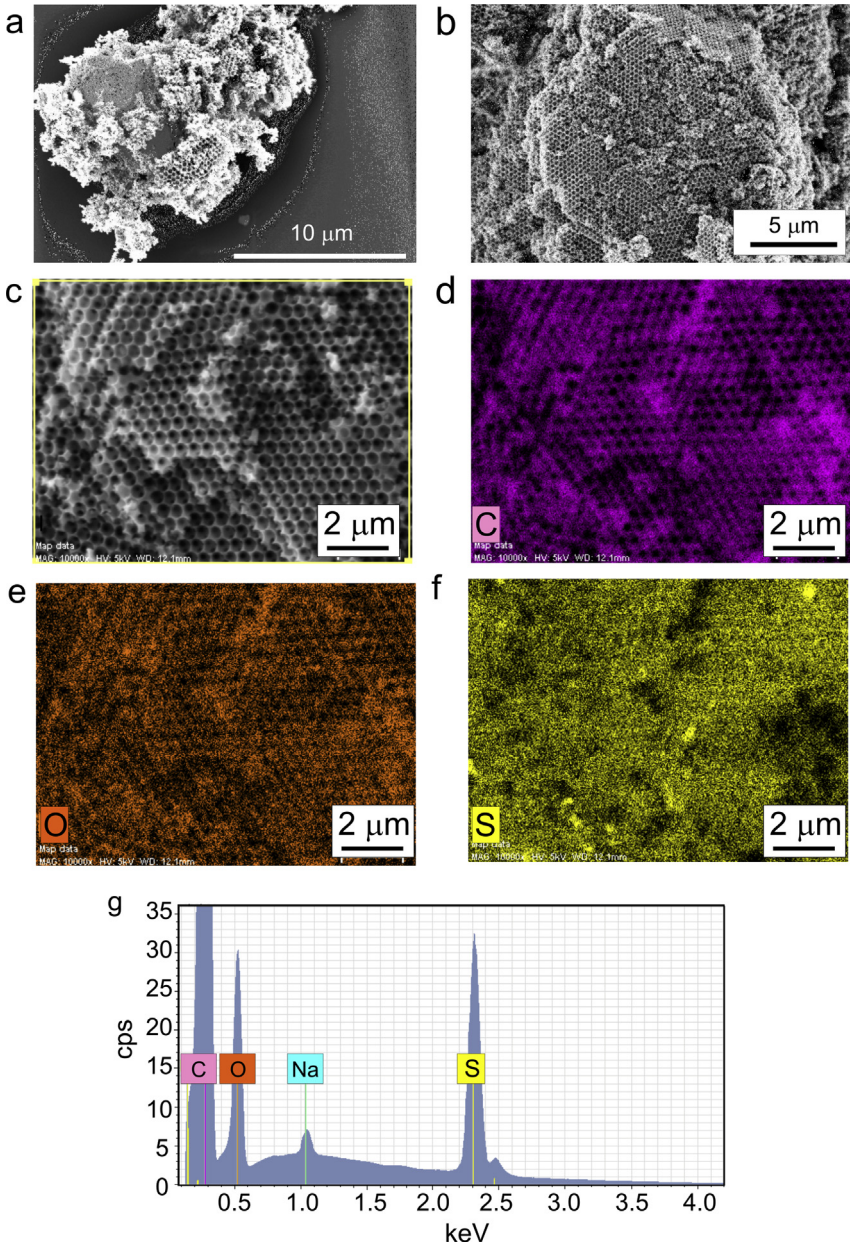

Fig. 5. SEM images of carbon electrode after mixing with sulfur (a), after annealing at 155 °C (b) for sample with 490 nm large pores. SEM image (c) and corresponding elemental maps obtained by EDX of sulfur-filled porous carbon matrix: (d) – carbon map; (e) - oxygen map; (f) – sulfur map; (h) – EDX spectra of the area marked by the yellow rectangle in (c) measured with sample with 490 nm large pores. (For interpretation of the references to color in this figure legend, the reader is referred to the web version of this article.)

measured between two electrodes situated on top of the piston and on the bottom of the cylinder by DMM 2001 Keithley Instruments. Basically, this is a two probe system. The conductivity derived from the resistance and the geometry data was then recorded against the pressure. The control of the device as well as the data acquisition and analysis was carried out by a custom-made software developed with TestPoint™. The software allows user programming of different cycles and automatic control. The pressure between the electrodes was maintained up to a maximum value of 1 MPa to avoid rupturing of the carbon nanostructures.

3. Results and discussions

The porous carbon material was prepared using colloidal crystal arrays as sacrificial template, formed by densely packed monodisperse PMMA colloidal particles synthesized by emulsion polymerization. Briefly, the particles were assembled from their aqueous dispersion by using centrifugation sedimentation to form closely packed opal-like structure (Fig. 1(a), Fig. 2(a,b)). The obtained opal-like structure was filled with resorcinol–formaldehyde resin (Fig. 1(b) and Fig. 2(c,d)), which was completely crosslinked and carbonized during heat treatment at high temperature treatment led, on one hand, to carbonization of the filled resin and, on the other hand, to decomposition and removal of PMMA particles. As result, porous carbon inverse-opal scaffold was formed (Fig. 1(c) and Fig. 2(e,f)). The formed material is highly brittle black powder.

The surface area of formed carbonized scaffolds was investigated using BET measurements (Fig. 3(a), Table 1). The fabricated porous carbon exhibit a type H3 hysteresis loop according Brunauer–Deming–Deming–Teller (BDDT) classification, indicating the presence of mesopores (2–50 nm). The initial rise in the curve (at $P/P0 < 0.05$) is associated with micropore filling. The low slope region in the middle of the isotherm from $P/P0 \approx 0.05$ to the starting point of the closed loop indicates multilayer adsorption on external surfaces including mesopores and macropores. The micropores with size around 1 nm were observed for all samples small fraction of mesopores with pore size in the range 2–50 nm were detected (Fig. 3(b)). The maximum of surface area was observed for the samples formed by 740 nm large particles, $S = 1340\ m^2\ g^{-1}$. The surface area of carbon formed by 490 nm large particles was close to $S = 700–800\ m^2\ g^{-1}$. Since the formed scaffold has highly periodic structures, there is the possibility to estimate area by considering the geometry of the inverse opal. The theoretical surface area was estimated using Eq. (1) by considering the geometry of inverse opal without considering the surface area of carbon itself:

$$S = \frac{6d}{(1-d)D\rho_C}, \tag{1}$$

where d is the volume fraction occupied by spheres $d = \pi/3\sqrt{2} \approx 0.74$ (where D is the particle diameter, ρ_c is mass density of carbon ($\rho_c \approx 2\ g\ cm^{-3}$). The surface area of scaffolds formed by smaller particles is considerably smaller than the predicted values that can be explained by multiple defects in the scaffold structure. The surface area of the scaffolds formed by largest particles is slightly higher than the predicted value that can

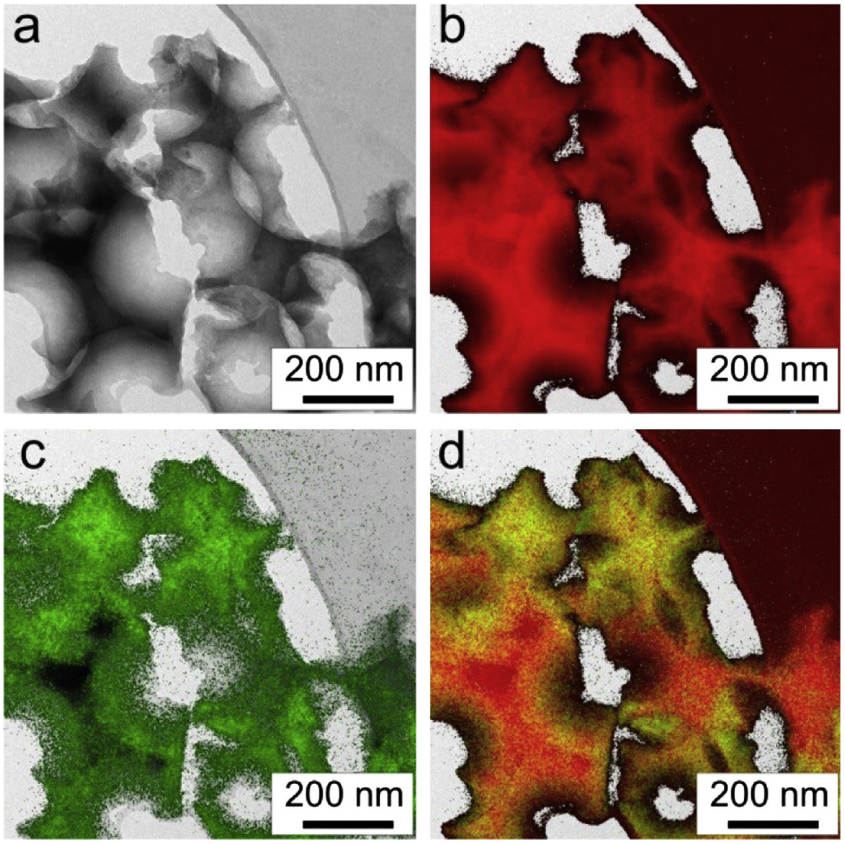

Fig. 6. TEM image (a) of sulfur filled carbon electrode and the corresponding elemental maps: (b) – carbon map and (c) sulfur map obtained by EFTEM; (d) overlap of carbon and sulfur maps measured with sample with 490 nm large pores.

be explained by formation of smaller pores during carbonization with diameter ca 1 nm as measured with BET. Important the surface area of all samples considerably exceeds surface area of CNTs, which is typically, less than 350 $m^2 g^{-1}$ [41] and is close to "super-microporous" ones (1473 $m^2 g^{-1}$ [25]) with the size of pores smaller than 3 nm.

We tested conductivity on the example of the porous carbon prepared using the particles of both sizes (490 and 740 nm). It was found that obtained carbon has high conductivity, which is around 600–900 mS cm^{-1} (Table 2). To compare its value of conductivity highly conducting lithium ion grade carbon black from TIMCAL Graphite and Carbon (Super P® Li) and mesoporous carbon from Sigma Aldrich (MPC- Sigma) were measured keeping the same experimental conditions. Interestingly, the conductivity of our carbon lies about 1/5th of the conductivity value obtained from Super P® Li, whereas the mesoporous carbon from Sigma Aldrich (MPC- Sigma) found to be non- conducting even at 30 MPa pressure. Thus, the carbon material derived from our approach found to have substantial value of conductivity sufficient for maintaining electrical contact between carbon and sulfur.

Next we investigated the chemical structure of formed porous carbon using XPS and Raman spectroscopy. As it was found using XPS (Fig. 4), formed material consists of carbon and contains considerable amount of oxygen (atomic ratio [O]:[C] = 0.157). The high-resolution C 1s spectrum clearly shows that formed carbon is 95% graphite (component peak *Gr* at 284 eV Table 2). The shift of position of carbon peak to lower energy (C 1s peak of saturated hydrocarbons is 285.00 eV) can be explained by the high electron density in conjugated π-electron systems [42]. The four wide shake-up peaks named result from electron transitions between π and π* orbitals in the conjugated ring systems of the graphitic lattices. Moreover there is ca 5% of carbon linked to oxygen through single bond that is most probably C–O groups, which can be considered as the result of surface oxidation processes taking place after the thermal treatment.

Raman spectra show peaks of both disordered amorphous carbon and graphite-like carbons with the ratio between area (A) of D ($\upsilon = 1344\ cm^{-1}$) and G ($\upsilon = 1596\ cm^{-1}$) bands A(D)/A(G) ≈ 2. The D-band represents sp^3 C–C bonds and the G-band planar sp^2 C–C bonds. Thus, based on the results of XPS and Raman spectroscopy, we can conclude that formed carbon is disordered graphite containing phenol groups.

Next, we prepared sulfur-filled porous carbon cathodes. For this, powder of porous carbon was mixed with elemental sulfur (Fig. 5) where the sulfur particles are clearly recognized using electron microscopy (Fig. 5(a)). The mixture was treated at 155 °C, the temperature at which molten sulfur shows lowest viscosity and therefore should readily diffuse into the pores of the carbon material. The homogeneity of filling was investigated by using SEM, EELS and EDX. First, no sulfur particles were observed in SEM analysis after melting (Fig. 5(b)). Second, elemental maps of carbon and sulfur obtained using EDX (Fig. 5(c–h)) and EELS (Fig. 6) clearly indicate on homogeneity of distribution of sulfur inside carbon matrix. Interestingly in EDX we observed peak of intrinsic to Na, whose appearance can be explained by considering conditions of preparation of porous carbon. Sodium carbonate was used as catalyst for crosslinking of resorcinol–formaldehyde resin. So, the peak or area of sodium in the EDX map originates from the amount of sodium left inside the composite material.

Finally, the electrochemical properties of porous carbon-sulfur cathodes were tested by means of cyclovoltammetric and galvanostatic charge/discharge measurements (Fig. 7(a)). During discharge (lower curves in Fig. 7(a)) the characteristic two reduction peaks at around 2.4 V and 2.0 V occur. As often discussed in literature, these peaks correspond to the reduction of sulfur to Li_2S_n ($n > 4$) and the subsequent reduction of higher

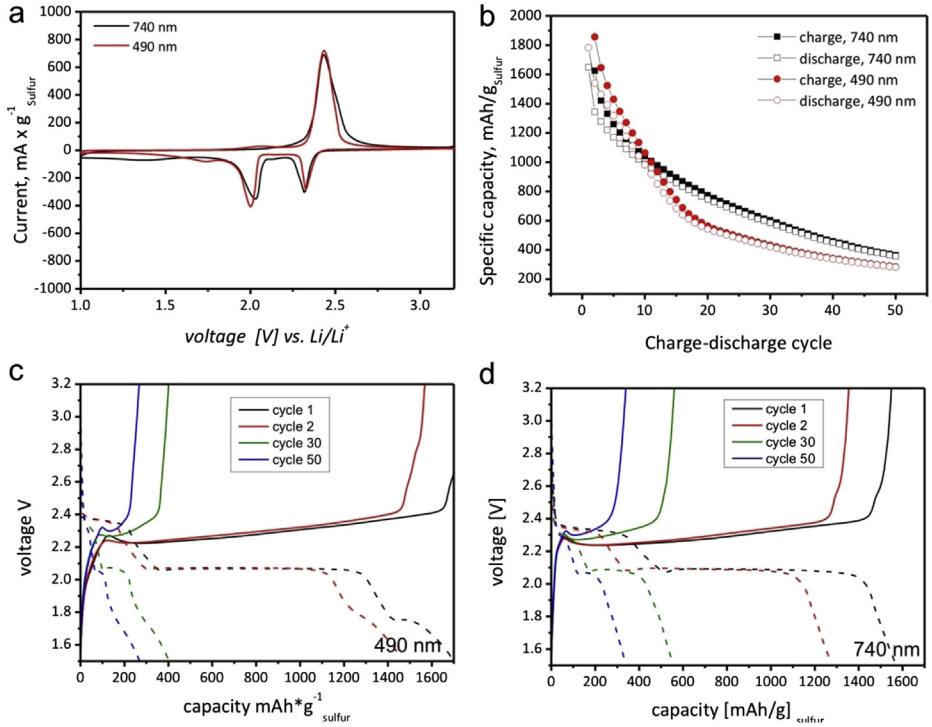

Fig. 7. Cycolvoltammetric (a) and charge/discharge measurements (b) of Li–S batteries assembled using cathodes with carbon materials obtained of 490 nm and 740 nm PMMA particles. (c,d) – constant current measurements of batteries with cathodes prepared using 490 nm (c) and 740 nm (d) large particles.

order polysulfides to short chain polysulfide species respectively. [43] In case of the sample obtained with 490 nm diameter PMMA particles an additional peak at 1.7 V occurs which should be related to the reduction of polysulfide species to form Li_2S [44]. The charging curve (upper curves in Fig. 7(a)) of the battery is represented by typical single peak at around 2.4 V. The relatively narrow peaks indicate good reaction kinetics for reduction as well as the oxidation reaction in the first cycle and run in a comparable range for both samples. The third reduction peak occurring at 1.7 V of the 490 nm sample, shows a rather broad shape which is clearly the consequence of slower reaction kinetics for Li_2S formation.

Fig. 7(b) shows the galvanostatic charge/discharge curves (calculated on gram sulfur) over the first 50 cycles and the corresponding voltage profiles in 7c/d. The initial discharge capacities of both samples run in the range of the theoretical specific capacity of sulfur; the exceeding capacity in the first cycle of the 490 nm sample may be due to residues of the carbon material production. Both types of cathodes are plagued with rapid capacity fading, especially over the first 10 to 15 cycles. The high initial capacity was reached because of the high surface area of the carbon materials and the resulting high contact area to otherwise electrically insulating sulfur. Nevertheless it is clearly a result of the very small electrode mass loading. The thin electrodes facilitate the accessibility of sulfur by electrolyte and also cause a relatively high ratio of the composite loading which gets in contact with the current collector. In the first cycles capacity fading is more pronounced. After 50 cycles the sample which was obtained by 740 nm PMMA particles shows a remaining discharge capacity of about 400 mAh g^{-1} sulfur or roughly a quarter of the theoretical discharge capacity of sulfur while the samples obtained by 490 nm PMMA particles retains a capacity of 300mAh g^{-1} sulfur. This may reflect the benefits of higher carbon surface area (obtained by the formation of 1 nm pores during carbonization) on the one hand and the bimodal pore size in which larger pores may be beneficial to ensure accessibility of active material by the electrolyte after prolonged cycling, while small pores would be clogged and impede Li^+ transport into pores. The plateaus in the voltage profiles match with the peak voltages of the cyclic voltammogramms for reduction and oxidation. With ongoing cycling the voltage plateaus of both samples move towards lower potentials during discharge and towards higher potentials during charge which is the result of increasing overvoltage. Again for the 490 nm sample a third reduction peak occurs at around 1.7 V. Presuming a more complete reduction of the sulfur species to solid Li_2S this additional plateau could explain the higher discharge capacity during the first cycles. However it may also cause more rapid capacity degradation as the oxidation of Li_2S to Li_2S_2 is a solid–solid reaction and may occur incomplete [45].

4. Conclusions

We developed a new route for synthesis of porous carbon materials, which are highly promising as carbon materials for cathodes in Li–S batteries. The porous carbon materials have very high surface areas, which are combined with interconnectivity of the pores. The sulfur cathode based on the prepared carbon demonstrates very high charge/discharge capacity during initial cycles that makes it very promising and it indicates very high utilization of active material i.e. sulfur. The capacity however fades during cycling and become relatively low in comparison to reported in literature [21,35,46,47], that is most probably related to polysulfide shuttle. The next efforts will be focused on the reduction of the rapid decrease of the capacity during cycling caused by polysulfide shuttle.

Acknowledgment

The authors are thankful to Dr. Bernd Schumann (Robert-Bosch GmbH) for fruitful discussions and German Research Foundation DFG (SPP 1473) for financial support.

References

[1] B. Dunn, H. Kamath, J.M. Tarascon, Science 334 (2011) 928–935.
[2] F.T. Wagner, B. Lakshmanan, M.F. Mathias, J. Phys. Chem. Lett. 1 (2010) 2204–2219.
[3] P. Simon, Y. Gogotsi, Nat. Mater. 7 (2008) 845–854.
[4] F.Y. Cheng, J. Liang, Z.L. Tao, J. Chen, Adv. Mater. 23 (2011) 1695–1715.
[5] J.B. Goodenough, Y. Kim, Chem. Mater. 22 (2010) 587–603.
[6] B. Scrosati, J. Garche, J. Power Sources 195 (2010) 2419–2430.
[7] A. Manthiram, J. Phys. Chem. Lett. 2 (2011) 176–184.
[8] M.S. Whittingham, Chem. Rev. 104 (2004) 4271–4301.
[9] B.L. Ellis, K.T. Lee, L.F. Nazar, Chem. Mater. 22 (2010) 691–714.
[10] B. Scrosati, J. Hassoun, Y.K. Sun, Energy Environ. Sci. 4 (2011) 3287–3295.
[11] P.G. Bruce, S.A. Freunberger, L.J. Hardwick, J.M. Tarascon, Nat. Mater. 11 (2012) 19–29.
[12] J. Chen, F.Y. Cheng, Acc. Chem. Res. 42 (2009) 713–723.
[13] X.L. Ji, L.F. Nazar, J. Mater. Chem. 20 (2010) 9821–9826.
[14] P.G. Bruce, B. Scrosati, J.M. Tarascon, Angew. Chem. Int. Ed. 47 (2008) 2930–2946.
[15] X. He, W. Pu, J. Ren, L. Wang, J. Wang, C. Jiang, C. Wan, Electrochim. Acta 52 (2007) 7372–7376.
[16] B. Zhang, C. Lai, Z. Zhou, X.P. Gao, Electrochim. Acta 54 (2009) 3708–3713.
[17] S. Dorfler, M. Hagen, H. Althues, J. Tubke, S. Kaskel, M.J. Hoffmann, Chem. Commun. 48 (2012) 4097–4099.
[18] J.-j. Chen, Q. Zhang, Y.-n. Shi, L.-l. Qin, Y. Cao, M.-s. Zheng, Q.-f. Dong, Phys. Chem. Chem. Phys. 14 (2012) 5376–5382.
[19] B. Wang, K. Li, D. Su, H. Ahn, G. Wang, Chem. Asian J. 7 (7) (2012) 1637–1643.
[20] Y. Cao, X. Li, I.A. Aksay, J. Lemmon, Z. Nie, Z. Yang, J. Liu, Phys. Chem. Chem. Phys. 13 (2011) 7660–7665.
[21] X. Ji, K.T. Lee, L.F. Nazar, Nat. Mater. 8 (2009) 500–506.
[22] Y. Yang, G. Yu, J.J. Cha, H. Wu, M. Vosgueritchian, Y. Yao, Z. Bao, Y. Cui, ACS Nano 5 (2011) 9187–9193.
[23] R. Elazari, G. Salitra, A. Garsuch, A. Panchenko, D. Aurbach, Adv. Mater. 23 (2011) 5641–5644.
[24] S. Flandrois, B. Simon, Carbon 37 (1999) 165–180.
[25] C. Lai, X.P. Gao, B. Zhang, T.Y. Yan, Z. Zhou, J. Phys. Chem. C 113 (2009) 4712–4716.
[26] M.M. Rao, W.S. Li, E.J. Cairns, Electrochem. Commun. 17 (2012) 1–5.
[27] L. Ji, M. Rao, S. Aloni, L. Wang, E.J. Cairns, Y. Zhang, Energy Environ. Sci. 4 (2011) 5053–5059.
[28] X. Li, Y. Cao, W. Qi, L.V. Saraf, J. Xiao, Z. Nie, J. Mietek, J.-G. Zhang, B. Schwenzer, J. Liu, J. Mater. Chem. 21 (2011) 16603–16610.
[29] B. Zhang, X. Qin, G.R. Li, X.P. Gao, Energy Environ. Sci. 3 (2010) 1531–1537.
[30] G. He, X. Ji, L. Nazar, Energy Environ. Sci. 4 (2011) 2878–2883.
[31] N. Jayaprakash, J. Shen, S.S. Moganty, A. Corona, L.A. Archer, Angew. Chem. Int. Ed. 50 (2011) 5904–5908.
[32] C. Liang, N.J. Dudney, J.Y. Howe, Chem. Mater. 21 (2009) 4724–4730.
[33] G. Zheng, Y. Yang, J.J. Cha, S.S. Hong, Y. Cui, Nano Lett. 11 (2011) 4462–4467.
[34] H. Wang, Y. Yang, Y. Liang, J.T. Robinson, Y. Li, A. Jackson, Y. Cui, H. Dai, Nano Lett. 11 (2011) 2644–2647.
[35] J. Schuster, G. He, B. Mandlmeier, T. Yim, K.T. Lee, T. Bein, L.F. Nazar, Angew. Chem. Int. Ed. 51 (2012) 3591–3595.
[36] N. Tachikawa, K. Yamauchi, E. Takashima, J.-W. Park, K. Dokko, M. Watanabe, Chem. Commun. 47 (2011) 8157–8159.
[37] S. Lee, Y. Lee, D.H. Kim, J.H. Moon, ACS Appl. Mater. Interfaces 5 (2013) 12526–12532.
[38] W. Guo, M. Wang, W. Xia, L. Dai, Langmuir 29 (2013) 5944–5951.
[39] D.-Y. Kang, S.-O. Kim, Y.J. Chae, J.K. Lee, J.H. Moon, Langmuir 29 (2013) 1192–1198.
[40] Y. Kim, C.-Y. Cho, J.-H. Kang, Y.-S. Cho, J.H. Moon, Langmuir 28 (2012) 10543–10550.
[41] J.J. Niu, J.N. Wang, Y. Jiang, L.F. Su, J. Ma, Microporous Mesoporous Mater. 100 (2007) 1–5.
[42] R.M. Novais, F. Simon, P. Pötschke, T. Villmow, J.A. Covas, M.C. Paiva, J. Polym. Sci. A Polym. Chem. 51 (2013) 3740–3750.
[43] K. Kumaresan, Y. Mikhaylik, R.E. White, J. Electrochem. Soc. 155 (2008) A576–A582.
[44] L. Ji, M. Rao, H. Zheng, L. Zhang, Y. Li, W. Duan, J. Guo, E.J. Cairns, Y. Zhang, J. Am. Chem. Soc. 133 (2011) 18522–18525.
[45] S.E. Cheon, K.S. Ko, J.H. Cho, S.W. Kim, E.Y. Chin, H.T. Kim, J. Electrochem. Soc. 150 (2003) A800–A805.
[46] R. Xu, I. Belharouak, J.C.M. Li, X. Zhang, I. Bloom, J. Bareño, Adv. Energy Mater. 3 (7) (2013) 833–838.
[47] B. Ding, C. Yuan, L. Shen, G. Xu, P. Nie, X. Zhang, Chemistry 19 (2013) 1013–1019.
[48] D.A. Shirley, Phys. Rev. B 5 (1972) 4709.